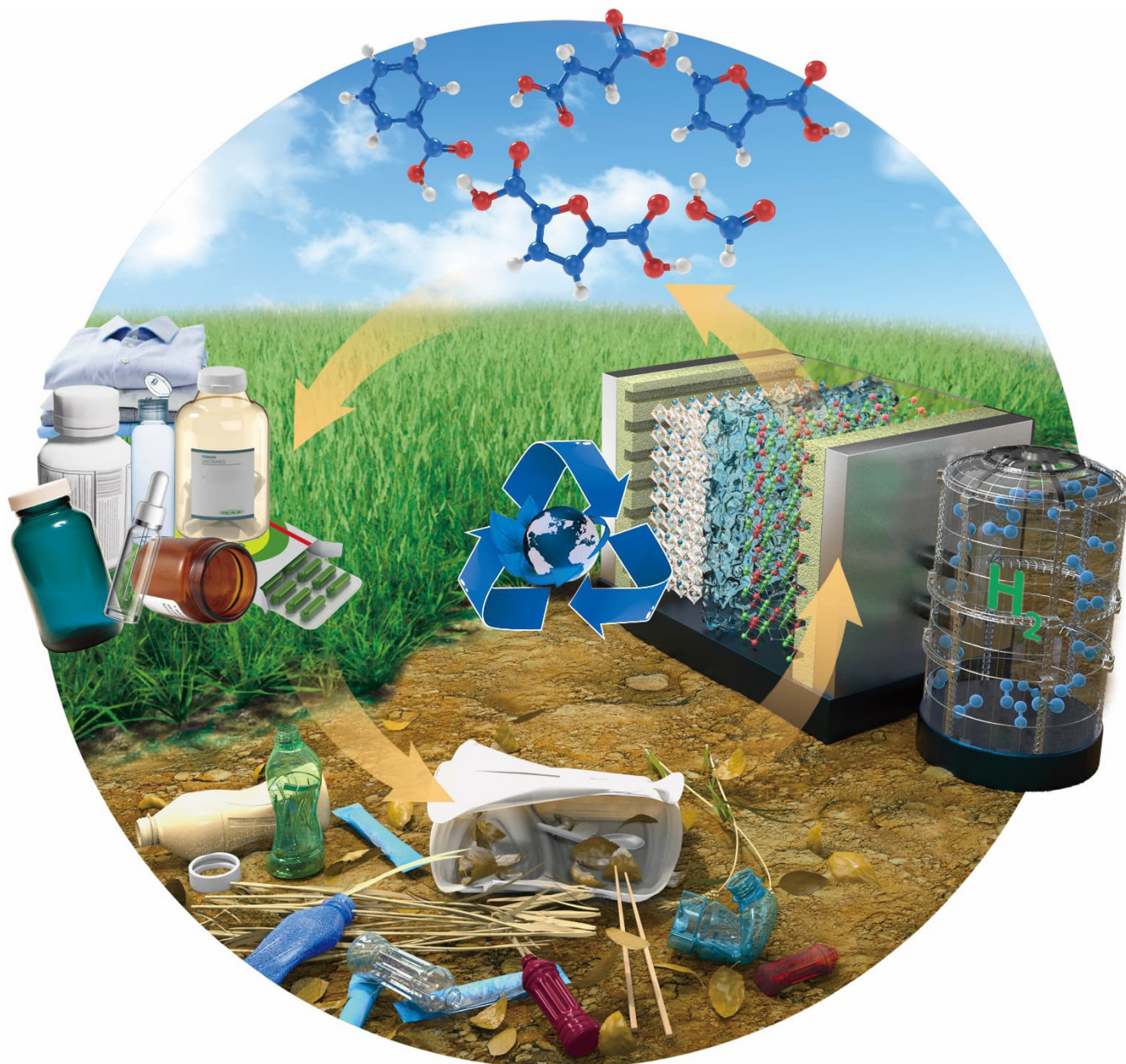


Hydrogen Evolution

How to cite: *Angew. Chem. Int. Ed.* **2023**, *62*, e202215804

International Edition: doi.org/10.1002/anie.202215804

German Edition: doi.org/10.1002/ange.202215804

A Novel Electrode for Value-Generating Anode Reactions in Water Electrolyzers at Industrial Current Densities*Changlong Wang, Yufeng Wu,* Alexander Bodach, Moritz Lukas Krebs, Wolfgang Schuhmann, and Ferdi Schüth**

Abstract: Hydrogen generated in electrolyzers is discussed as a key element in future energy scenarios, but oxygen evolution as the standard anode reaction is a complex multi-step reaction requiring a high overpotential. At the same time, it does not add value—the oxygen is typically released into the atmosphere. Alternative anode reactions which can proceed at similar current densities as the hydrogen evolution are, therefore, of highest interest. We have discovered a high-performance electrode based on earth-abundant elements synthesized in the presence of H₂O₂, which is able to sustain current densities of close to 1 A cm⁻² for the oxidation of many organic molecules, which are partly needed at high production volumes. Such anode reactions could generate additional revenue streams, which help to solve one of the most important problems in the transition to renewable energy systems, i.e. the cost of hydrogen electrolysis.

Global energy systems are shifting increasingly from fossil resources towards renewable energy, which is mostly harvested in the form of electrical energy via wind or photovoltaics.^[1] However, storage of electrical energy is difficult on the grid scale, and the infrastructure for electricity transmission from sun-rich parts of the world to regions with high energy consumption is lacking.^[2] Thus, both for storage and transportation, conversion of part of the harvested electrical energy to a high energy content chemical is a preferred solution,^[3] and this approach is an important element of the energy strategy in many countries. Hydrogen is the most obvious choice for the initially generated chemicals since the technology for water electrolysis is commercially available and rather efficient.^[4]

While it is a technologically viable solution, hydrogen from water electrolysis suffers from a severe cost problem.^[5] Depending on local conditions and technology implemented, fossil hydrogen is produced at roughly 1 €/kg H₂, mostly by natural gas steam reforming, although the price has recently

increased substantially due to strongly increasing natural gas prices in parts of the world. This cost will increase with increasing CO₂ pricing. In contrast, electrolytic hydrogen,^[6] again depending on local conditions, predominantly on the price of electricity and capital expense for electrolyzers, is currently at best at around 3 \$/kg,^[7a] but projections see it at about 1 \$/kg in the future.^[7b,c] Moreover, in the electrolyzer, the bottleneck is the oxygen evolution reaction at the anode,^[8] which is rather sluggish and results in a zero-value product, oxygen, which is released into the atmosphere.

Realizing alternative anode reactions,^[9] which produce valuable chemicals preferentially at lower overpotentials, could provide an additional revenue stream. Moreover, if such an alternative anode reaction proceeds easily at low overpotential, expensive catalysts could be replaced, and the electrolysis would run more efficiently. Technologically, there is one such process already operating on a large technical scale, i.e. chlorine production, where in fact, chlorine formed at the anode is the most valuable product, and the cathodically formed hydrogen is only a welcome by-product. However, for such alternative anode reactions, it is crucial that they run at similarly high current densities as the hydrogen evolution, i.e. at several hundred mA cm⁻² (alkaline electrolyzer) to more than 1 A cm⁻² (PEM electrolyzer).

We have systematically explored suitable catalysts for anode reactions, which have the potential for bulk production volumes. The oxidation of biomass-based 5-hydroxymethylfurfural (HMF) to furandicarboxylic acid (FDCA) is such a reaction^[10–13] because FDCA could replace the terephthalic acid in polyethyleneterephthalate (PET), a bulk polymer produced at a level of about 60 million tons annually (2015) with high growth rate.^[14] Catalysts should be selected from abundant metals for sustainability and cost reasons if sufficiently high activities could be achieved. There is a number of reports on the electrooxidation of HMF to FDCA on different electrodes, some of rather complex nature, achieving current densities ranging from a few ten to hundreds mA cm⁻², (for a survey, see Table S1), which are, however, often difficult to compare.^[15] Electrolysis at either high current density (> 300 mA cm⁻²) or high HMF concentrations for efficient and selective FDCA synthesis approaching industrial conditions remains less explored.

Nickel foam has been described as a suitable basis for anodes under alkaline conditions. It is known that the activity of iron-modified nickel for the oxygen evolution reaction is strongly enhanced.^[16] Increased activity is observed even if pure nickel electrodes are used in an alkaline electrolyte since iron contaminations typically present in KOH are deposited on the nickel electrode and enhance performance.^[17] This was the starting point of the development of electrodes made from highly earth-abundant elements, which allow the electrooxidation of different substrates, foremost HMF, at current densities of industrial electrolyzers for hydrogen production. It was found that dipping a nickel foam electrode in a solution of FeCl₃·6H₂O (Supporting Information, experimental section) already improved the performance of the electrode for the oxidation of HMF to FDCA substantially (Figure S2). However, a key

[*] Dr. C. Wang, Dr. A. Bodach, M. L. Krebs, Prof. Dr. F. Schüth
MPI für Kohlenforschung
Kaiser-Wilhelm-Platz 1, 45470 Mülheim (Germany)
E-mail: schueth@kofo.mpg.de

Dr. C. Wang, Prof. Dr. Y. Wu
Institute of Circular Economy, Faculty of Materials and Manufacturing, Beijing University of Technology
Beijing 100124 (P. R. China)
E-mail: wuyufeng3r@126.com

Prof. Dr. W. Schuhmann
Analytical Chemistry-Center for Electrochemical Sciences (CES);
Faculty of Chemistry and Biochemistry, Ruhr University Bochum
Universitätsstr. 150, 44780 Bochum (Germany)

© 2022 The Authors. Angewandte Chemie International Edition published by Wiley-VCH GmbH. This is an open access article under the terms of the Creative Commons Attribution Non-Commercial NoDerivs License, which permits use and distribution in any medium, provided the original work is properly cited, the use is non-commercial and no modifications or adaptations are made.

improvement in the electrode performance was achieved if the iron chloride was not dissolved in water but in 5 wt% H_2O_2 solution to reach a concentration of 2.5 mM. This improved synthesis takes advantage of a Fenton-like reaction between Fe^{3+} and H_2O_2 , producing strong oxidative hydroxy radicals. This facilitates the corrosion of nickel foam, releasing Ni^{2+} species into the solution, which react spontaneously with Fe^{3+} , OH^- and soluble CO_3^{2-} to form NiFe-LDH on the nickel foam surface.^[18] On the other hand, excess Fe^{3+} reacts with OH^- to produce $\alpha\text{-FeOOH}$, which interfacially interacts with the NiFe-LDH via bridging oxygens,^[18d] forming active NiFe-LDH/ $\alpha\text{-FeOOH}$ heterostructures (see below). As a result, a nickel foam electrode modified with iron in such a solution for just one minute reached a current density of above 500 mA cm^{-2} at a potential of 1.478 V (vs. RHE) at an HMF concentration of 50 mM (Figure 1 and Figure S4), which is compatible with cathodic current densities in alkaline electrolyzers.

The potential for oxygen evolution is sufficiently more positive compared to HMF oxidation (Figure 1a) that FDCA can be produced almost without oxygen evolution as a competing reaction. The overpotential of electrochemical oxidation of HMF coincides with the potential of the transition from $\text{Ni}^{2+} \rightarrow \text{Ni}^{3+}$, and a rapid current increase was observed after this transition. This indicates that HMF oxidation is mediated by the oxidation of the Ni species to higher oxidation states in the oxyhydroxide, especially taking into account that the applied potential during HMF oxidation is more positive than that of the $\text{Ni}^{2+}/\text{Ni}^{3+}$ transition. This agrees well with findings for NiOOH catalysts,^[19] although the doping with transition metal

cations (e.g., Co and Fe) would substantially influence the position of the reaction overpotential.^[19a] Two mechanisms are proposed for this reaction; one hypothesis is the indirect oxidation mechanism involving chemical hydrogen atom transfer to Ni^{3+} sites, while the other hypothesis relies on a potential-dependent oxidation mechanism involving electrochemically induced hydride transfer to Ni^{4+} sites.^[19b] The mechanism could probably be clarified by in situ studies of the electrode surface, which, however, are beyond the scope of this study. In Figure 1c, the concentration of HMF, FDCA, and the intermediates are plotted over the charge passed in chronoamperometric experiments where samples were taken at regular intervals. As one can notice, the concentration of the intermediates is always low, which suggests that the first oxidation step is the slowest one; then, the reaction proceeds rapidly to FDCA. FDCA can be formed by two pathways,^[20] i.e. oxidation of the hydroxymethyl-group first, which leads to the formation of diformylfuran (DFF), or oxidation of the formyl-group first, which leads to hydroxymethylfurancarboxylic acid (HMFCFA). HMFCFA is observed at a slightly higher concentration than DFF over time, which could suggest that the reaction proceeds predominantly via the HMFCFA pathway. On the other hand, DFF is not stable under the reaction conditions, so that also other pathways via side reactions are conceivable.

Interestingly, the carbon balance is well closed throughout the whole reaction. This is somewhat surprising at first sight since HMF is known to degrade under basic conditions. However, in a detailed study, we have demonstrated that HMF degrades initially via a Cannizzaro reaction, the products of which can also be oxidized to FDCA. This explains the puzzling and widely neglected fact that HMF can be electrooxidized with very high yields to FDCA in spite of its instability under alkaline conditions.^[21] The protons eliminated from the substrate are essentially fully used for cathodic H_2 generation. The measured pH drop during the reaction corresponds to the neutralization of the protons from the FDCA generated, resulting in formation of the carboxylate. Thus, overall the reaction can be carried out at a high chemical yield close to 100% and a high Faradaic efficiency close to 100%.

Based on the excellent performance of the anode at high current densities, conditions allowing high space-time-yields and approaching industrial conditions of such processes were explored. In the range of concentration and electrode surface area studied here, the reaction is first order in HMF concentration and electrode surface area (Figures S7 and S8), and thus in order to increase the current density further, HMF starting levels were increased to 100 mM. This allows high current density electrolysis at the initial current density of 862 mA cm^{-2} (Figure 1b and Supporting Information), with both FDCA yield and Faradaic efficiency at $>92\%$, using either NafionTM 117 as a proton-exchange membrane or Fumasep FAB-PK-130 as an anion-exchange membrane. However, the Nafion membrane results in a significant crossover of HMF/intermediates from the anode to the cathode chamber,^[12] so for practical purposes, the anion-exchange membrane is preferred (Figure S9). Moreover,

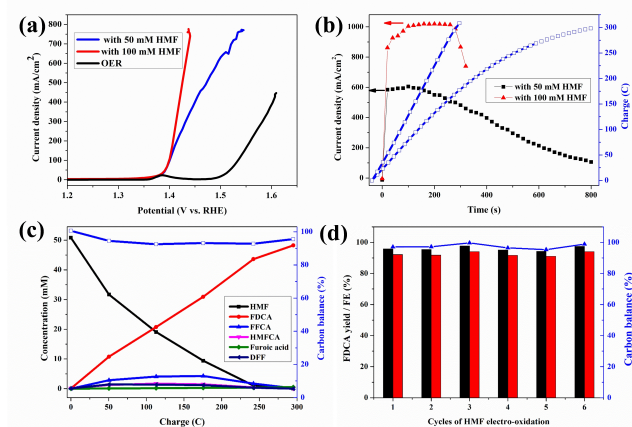


Figure 1. HMF electro-oxidation over a NiFe-1 electrode with different concentrations of HMF. a) LSVs (without iR compensation, results with 85% iR compensation are shown in Figure S6), b) current densities, charges vs. time curves, c) conversion and concentration changes of HMF and its oxidation products during the electrochemical oxidation of 50 mM HMF, and d) recyclability test: the FDCA yields (black column), Faradaic efficiencies (FE, red column) and carbon balance (blue) during 50 mM HMF electrooxidation. Reaction condition: 1 M KOH, 50 mM or 100 mM HMF, applied potential 1.478 V (vs. RHE). Current density is calculated by normalizing the current to geometrical surface area of the electrode (10 mm \times 10 mm, Supporting Information).

membrane stability issues over longer experiment times were also noticed under the strongly alkaline conditions (Figure S51 and explanation). The high current densities and low reaction times required for full conversion also suggest that the reaction can be carried out under single-pass flow-through conditions, which would facilitate the practical implementation of the oxidation process even further. Thus, a flow H-cell configuration was assembled, and the electrochemical synthesis of FDCA using 100 mM HMF was conducted at 1.478 V (vs. RHE, Figure 2a). Flow rate-current density dependencies were explored, and the best results were obtained with a Faradaic efficiency of 77–89 % to FDCA in a single pass at a flow rate of 0.4 mL min⁻¹ (Figure 2b). Moreover, since the *iR*-compensation has significant impact on the applied potentials for OER and HMF oxidations (Figure S6), optimized cell design would minimize the resistance, leading to improved current distribution and overall performance for the oxidation reactions of the different substrates.

In order to see whether the beneficial effect of hydrogen peroxide is restricted to iron on nickel foam or more broadly applicable, also other metals were studied, both as a modifier of the nickel foam and as metal foams as the basis of the electrode. The modified metal foams all showed enhanced performance in HMF electrooxidation compared to the untreated counterparts, suggesting that the use of hydrogen peroxide is more generally applicable in the fabrication of advanced and high-performance electrodes (Supporting Information section 5). Particularly Cu-based electrodes appear to be promising as well in HMF electrooxidation, showing high current density at a slightly higher

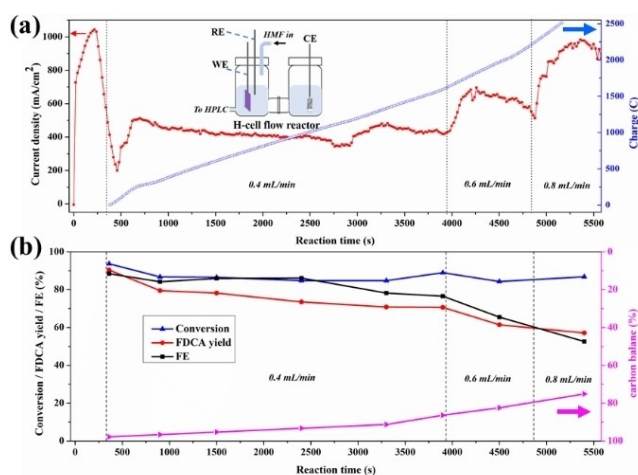


Figure 2. HMF electro-oxidation over NiFe-1 electrode in a flow H-cell configuration. a) Current densities, charge vs. time curves. Inset shows a cartoon of the H-cell configuration used for single pass flow-through reaction (WE, working electrode; RE, reference electrode; CE, counter electrode; HPLC, high-performance liquid chromatography). b) HMF conversion, FDCA yield, FE and carbon balance during the flow cell HMF electro-oxidation. All electrochemical tests are conducted in 1 M KOH with 100 mM HMF at the applied potential 1.478 V (vs. RHE) in an aqueous H-cell configuration

potential than that of the NiFe-1 electrode (Supporting Information section 5.2.3).

In electrochemistry, the question of whether a modification of the electrode increases the intrinsic site activity or only increases the electrochemically active surface area (ECSA), determined from the non-faradaic double-layer capacitance (Supporting Information section 6), is important for a better understanding of the relevant processes.^[8a] The ECSA-normalized electrochemical performance of the NiFe-1 electrode is the highest, together with the smallest charge transfer resistance compared with other samples as obtained from electrochemical impedance spectroscopy (EIS). Hence NiFe-1 is intrinsically more active. These results indicate that an increased number of active sites are created by the addition of FeCl₃·6H₂O in H₂O₂.

In order to trace back the improved performance of the NiFe-1 electrode, the surfaces of both the Ni foam electrode and Ni foil control electrodes were analyzed. The freshly synthesized NiFe-1 electrode shows a slightly yellowish color, and the originally smooth metal surface becomes rough due to the formation of high-density nanosheet-like units, which are well oriented with a high concentration of edges, boundaries, and defects (Figures 3a, b and Supporting Information section 7). The HAADF-STEM images clearly show the nanosheet-like structures with a thickness of 1.4 ± 0.2 nm (Figure 3c), which are additionally confirmed by AFM (Figure S58). Elemental mapping images suggest homogeneous distribution of Fe, Ni, O, and C, confirming the introduction of Fe species in the surface layer of the NiFe-1 electrode (Figures S59 and S60). In the whole NiFe-1 electrode, the iron content is 230 ppm (wt/wt), determined by AAS. However, it is not possible to determine the loading of the active catalyst, mainly due to the complexity of the synthetic processes and the fact that the nature of the real active catalyst is not clear.

XPS data (Figure S61) suggest Ni^{II} species resembling Ni(OH)₂,^[22] the energy of the iron signals corresponds to Fe^{III}, with the spectra resembling Fe(OH)₃. A shoulder at

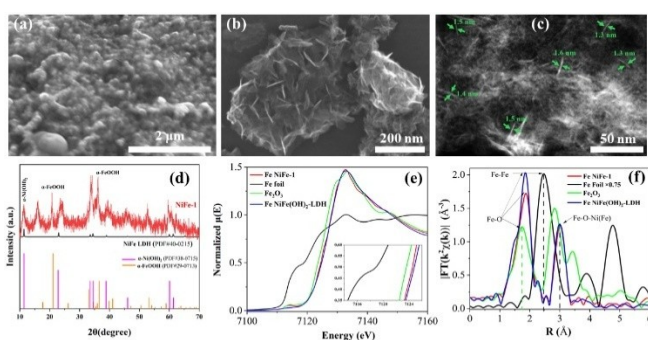
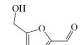
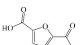
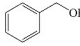
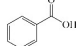
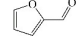
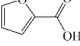
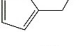
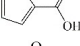
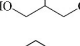
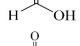
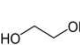
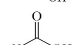
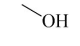
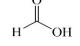
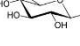
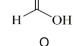
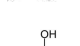
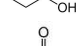
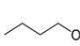
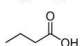
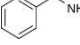
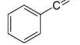


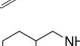
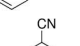
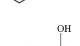
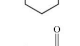
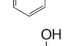
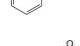
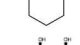

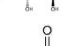

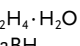

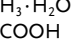
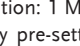


Figure 3. Characterizations of the NiFe-1 electrode. a) SEM image of the NiFe-1 electrode; b) Secondary electron image of the nanosheets ultrasonically peeled from the NiFe-1 electrode; c) HAADF-STEM image shows the nanosheet-like units with different thickness; d) XRD; e) Normalized Fe K-edge X-ray absorption near-edge structure (XANES) $\chi(E)$ spectra, and f) radial distance $\chi(R)$ space spectra. (Reference samples: Fe foil, Fe₂O₃, and pristine NiFe layered double hydroxide nanosheets (NiFe-LDH)).

Table 1: Electrochemical oxidative upgrading of organic molecules.^[a]

Entry	substrate	product	Current density ^[b] [mA cm ⁻²]	Product yield ^[c] [%]	Carbon balance [%]	FE [%]
1			862	92	97	92
2			723	94	102	92
3			756	97	103	96
4			855	96	98	94
5			669	96	91	88
6			634	87	94	82
7			632	99	84	82
8			757	81	81	77
9			841	99	87	86
10			479	84	97	84
11			236	89	96	86
12			699	77	91	74
13			814	94	94	96
14			651	86	86	86
15			612	85	96	85
16			585	88	88	88
17			351	74	88	75
18			292	77	71	78
19 ^[d]		–	613	–	–	–
20 ^[e]		–	791	–	–	–
21 ^[e]	N ₂ H ₄ · H ₂ O	–	1420	–	–	–
22 ^[e]	NaBH ₄	–	727	–	–	–
23 ^[f]	NH ₃ · H ₂ O	–	–	–	–	–
24 ^[f]	HCOOH	–	–	–	–	–

[a] Reaction condition: 1 M KOH, 100 mM substrates in an H-cell and electrolysis at 1.478 V vs. RHE. [b] Measured at the initial reaction time of 20 s, as is already pre-settled by the system. [c] Yields calculated on the basis of HPLC and GC results. [d] We were not able to identify and quantify the products. [e] Ultra-high current density and fast kinetics are observed, but we could not identify and quantify the products. [f] No reaction. [g] Standard deviations for the yields and FEs are $\pm 2\%$.

288 eV in the carbon 1s peak might be attributed to carbonate species. The XRD pattern of the NiFe-1 sample measured with a rotating anode (Cu K α radiation) shows additional reflections consistent with nickel-iron carbonate hydroxide hydrate (PDF#40-0215) that possesses analogous structures to α -Ni(OH)₂.^[23] Moreover, strong reflections assigned to α -FeOOH also indicate the presence of this highly reactive iron-containing species^[24] in the NiFe-1

sample (Figure 3d). In order to further evaluate the chemical state and local structure of the NiFe-1, X-ray absorption fine structure measurements at the Fe K-edge, rather than the Ni K-edge due to the bad contrast to bulk Ni foam, were performed (Figures 3e, f, and S64, S64). The Fe K-edge X-ray absorption near-edge structure (XANES) spectrum showed binding and edge energies close to those of Fe₂O₃ and pristine NiFe-LDH samples, indicating the oxidation

state of Fe in the NiFe-1 electrode is about +3 (Figure 3e), in agreement with the XPS analysis. The Fourier transform (FT) of the $k^2\chi(k)$ into radial distance $\chi(R)$ at the Fe K-edge reveals substantial but less noticeable reductions in the peak densities for Fe–O and Fe–O–Ni/Fe–O–Fe path, respectively, compared to that of the pristine NiFe-LDH (Figure 3f). The average coordination numbers of Fe–O and Fe–O–Ni/Fe–O–Fe paths were 4 and 6, respectively. Those results suggest the presence of both oxygen vacancies and metal defects in the NiFe-1 electrode.

FDCA is a highly interesting molecule, which could reach production amounts in the range of multi-ten-million tons per year and thus be a suitable product for the anode reaction in hydrogen production units. Although this would only correspond to about 2% of the current global hydrogen demand, if synthesized at the scale of terephthalic acid, it could facilitate ramping up sustainable hydrogen production. Moreover, there are many other interesting oxidation products which could be synthesized anodically in conjunction with water electrolysis. Thus, a range of additional substrates was explored on the NiFe-1 electrode, and in most cases, also these substrates could be oxidized at similarly high current densities with high yields and high faradic efficiency (Table 1, Supporting Information section 8). Various primary amines are also efficiently and selectively oxidized to nitriles in water over the NiFe-1 anode (Table 1, entries 13–16). The phase separation, with the oily nitriles floating on the surface of the electrolyte, not only avoids blocking of the active sites but would also enable the continuous large-scale production/separation of nitriles with industrial practicability (Figures S81–S87).

In glucose electrooxidation, formic acid was identified as the final product instead of the expected gluconic acid (Table 1, entry 9), suggesting electrochemical oxidative C–C bond cleavage. This could have significance for the conversion of biobased substrates because carbohydrates and lignin, featuring C(OH)–C motifs, could be converted to carboxylic acids via selective C–C bonds cleavage.^[25] We thus chose the lignin-derived cyclohexanol as substrate (Table 1, entry 18), which was interestingly converted to adipate via cyclohexanone as the intermediate, as confirmed by HPLC analysis (Figure S89). Therefore, this electrochemical conversion offers a sustainable pathway for the large-scale, efficient, and selective production of adipic acid from renewable biomass substrates.^[26] Adipic acid is an important industrial intermediate to produce nylon 6,6 (polyester, plastic, etc.) and it is also used in the food and cosmetics industry.^[26] Moreover, hydrogen evolution at the anode side is also observed. Thus, hydrogen evolution at the cathode integrated with either electrooxidation of suitable substrates (e.g., aldehydes, cyclohexanol) or electro-half-oxidation of alcohols/aldehydes (e.g., Table 1, entries 3, 11, 17) in a controlled manner, could offer triple advantages: anodic and cathodic H₂ co-production, and anodic production of valuable organics.^[27] The potential of the electrodes was also explored for fuel cell-type reactions (Table 1, entries 20–23), and also their reactions delivered high current density and fast kinetics for gas evolution on this new type of electrode.

We have introduced a versatile method for the preparation of advanced nickel-based anodes with metal modification of the base material in the presence of H₂O₂. These electrodes sustain high current densities in the order of several hundreds up to over 1000 mA cm⁻² in the oxidation of various organic substrates at high selectivity for value-added products. These products are highly demanded in the industry, while the obtained current densities are in the order of technical processes. The presence of the organic substrates decreases the potential compared to oxygen evolution, which is an additional benefit. Moreover, the process can be carried out in a continuous fashion, principally allowing scale-up for bulk production of the target products. Given the high demand for some of the products studied, the discovery could be an element to substantially improve the economics of hydrogen production by electrolysis in an electrolyzer configuration, where cathodically hydrogen is evolved and anodically valuable products such as furandicarboxylic acid, adiponitrile, or adipic acid are synthesized.

Acknowledgements

We thank H. Bongard and N. Pfänder for electron microscopy analysis, S. Leiting and C. Weidenthaler for XPS measurements, J. Ternieden for XRD measurements, V. Dietl and S. Eichler for GC/GC-MS analysis, H. Hinrichs and M. Sterling for conducting the HPLC analysis, and fruitful discussions. We thank NSRRC for the synchrotron radiation beam time. Financial support from the Deutsche Forschungsgemeinschaft (DFG, German Research Foundation) under Germany's Excellence Strategy-Cluster of Excellence 2186 "The Fuel Science Center"-ID: 390919832 and FOR 2982-UNODE, Project number 413163866, National Key R&D Program of China (2021YFC2902505) and the start-up funding by Beijing University of Technology (C.W.) is gratefully acknowledged. Open Access funding enabled and organized by Projekt DEAL.

Conflict of Interest

The authors declare no conflict of interest.

Data Availability Statement

The data that support the findings of this study are available in the supplementary material of this article.

Keywords: Anodic Oxidation · FDCA · H₂O₂ · High Current Density · NiFe Electrode

[1] a) H. J. Snaith, *Nat. Mater.* **2018**, *17*, 372–376; b) M. Riede, D. Spoltore, K. Leo, *Adv. Energy Mater.* **2021**, *11*, 2002653.

[2] a) P. Albertus, J. S. Manser, *Joule* **2020**, *4*, 21–32; b) M. C. Argyrou, P. Christodoulides, S. A. Kalogirou, *Renewable*

- Sustainable Energy Rev.* **2018**, *94*, 804–821; c) Z. Zhu, T. Jiang, M. Ali, Y. Meng, Y. Jin, Y. Cui, W. Chen, *Chem. Rev.* **2022**, *122*, 16610–16751.
- [3] a) J. L. Barton, *Science* **2020**, *368*, 1181–1182; b) T. M. Gür, *Energy Environ. Sci.* **2018**, *11*, 2696–2767.
- [4] a) S. A. Grigoriev, V. N. Fateev, D. G. Bessarabov, P. Millet, *Int. J. Hydrogen Energy* **2020**, *45*, 26036–26058; b) Z. -Y. Yu, Y. Duan, X. -Y. Feng, X. Yu, M. -R Gao, S. -H Yu, *Adv. Mater.* **2021**, *33*, 2007100.
- [5] a) P. Nikolaidis, A. Poullikkas, *Renewable Sustainable Energy Rev.* **2017**, *67*, 597–611; b) J. N. Hausmann, R. Schlögl, P. W. Menezes, M. Driess, *Energy Environ. Sci.* **2021**, *14*, 3679–3685; c) T. Terlouw, C. Bauer, R. McKenna, M. Mazzotti, *Energy Environ. Sci.* **2022**, *15*, 3583–3602.
- [6] a) M. K. Debe, *Nature* **2012**, *486*, 43–51; b) Z. W. Seh, J. Kibsgaard, C. F. Dickens, I. Chorkendorff, J. K. Nørskov, T. F. Jaramillo, *Science* **2017**, *355*, eaad4998; c) S. Z. Oener, M. J. Foster, S. W. Boettcher, *Science* **2020**, *369*, 1099–1103.
- [7] a) S. van Renssen, *Nat. Clim. Change* **2020**, *10*, 799–801; b) “Hydrogen Shot,” U. S. Department of Energy, Accessed September 20, 2021; c) IRENA (2020), Green Hydrogen Cost Reduction: Scaling up Electrolysers to Meet the 1.5°C Climate Goal, International Renewable Energy Agency, Abu Dhabi. ISBN: 978-92-9260-295-6.
- [8] a) C. C. McCrory, S. Jung, I. M. Ferrer, S. M. Chatman, J. C. Peters, T. F. Jaramillo, *J. Am. Chem. Soc.* **2015**, *137*, 4347–4357; b) B. Zhang, L. Wang, Z. Cao, S. M. Kozlov, F. P. Garca de Arquer, C. T. Dinh, J. Li, Z. Wang, X. Zheng, L. Zhang, Y. Wen, O. Voznyy, R. Comin, P. De Luna, T. Regier, W. Bi, E. E. Alp, C.-W. Pao, L. Zheng, Y. Hu, Y. Ji, Y. Li, Y. Zhang, L. Cavallo, H. Peng, E. H. Sargent, *Nat. Catal.* **2020**, *3*, 985–992; c) C. Kuai, Z. Xu, C. Xi, A. Hu, Z. Yang, Y. Zhang, C.-J. Sun, L. Li, D. Sokaras, C. Dong, S.-Z. Qiao, X.-W. Du, F. Lin, *Nat. Catal.* **2020**, *3*, 743; d) X. Tian, X. Zhao, Y.-Q. Su, L. Wang, H. Wang, D. Dang, B. Chi, H. Liu, E. J. M. Hensen, X. W. Lou, B. Y. Xia, *Science* **2019**, *366*, 850–856; e) K. P. Gong, F. Du, Z. H. Xia, M. Durstock, L. M. Dai, *Science* **2009**, *323*, 760–764.
- [9] a) R. Li, K. Xiang, Z. Peng, Y. Zou, S. Wang, *Adv. Energy Mater.* **2021**, *11*, 2102292; b) G. Chen, X. Li, X. Feng, *Angew. Chem. Int. Ed.* **2022**, *61*, e202209014; *Angew. Chem.* **2022**, *134*, e202209014; c) H. Duan, F. Wang, *Chem Catalysis* **2022**, *2*, 641–643; d) Z. Li, X. Li, H. Zhou, Y. Xu, S.-M. Xu, Y. Ren, Y. Yan, J. Yang, K. Ji, L. Li et al, *Nat. Commun.* **2022**, *13*, 5009.
- [10] G. Grabowski, J. Lewkowsky, R. Skowronski, *Electrochim. Acta* **1991**, *36*, 1995.
- [11] H. G. Cha, K. S. Choi, *Nat. Chem.* **2015**, *7*, 328–333.
- [12] W. Liu, L. Dang, Z. Xu, H.-Q. Yu, S. Jin, G. W. Huber, *ACS Catal.* **2018**, *8*, 5533–5541.
- [13] a) B. You, Y. Sun, *Acc. Chem. Res.* **2018**, *51*, 1571–1580; b) C. Wang, H.-J. Bongard, C. Weidenthaler, Y. Wu, F. Schüth, *Chem. Mater.* **2022**, *34*, 3123–3132; c) C. Wang, H. -J Bongard, M. Yu, F. Schüth, *ChemSusChem* **2021**, *14*, 5199–5206.
- [14] a) E. Gubbels et al, *Ullmanns Handbook of Industrial Chemistry, online Edition, Polyesters*, Wiley, Hoboken, **2000**; b) C. Wang, H. Han, Y. Wu, D. Astruc, *Coord. Chem. Rev.* **2022**, *458*, 214422; c) H. Zhou, Y. Wang, Y. Ren, Z. Li, X. Kong, M. Shao, H. Duan, *ACS Catal.* **2022**, *12*, 9307–9324.
- [15] S. Wöllner, T. Nowak, G.-R. Zhang, N. Rockstroh, H. Ghanem, S. Rosiwal, A. Brückner, B. J. M. Etzold, *ChemistryOpen* **2021**, *10*, 600–606.
- [16] a) D. Y. Chung, P. P. Lopes, P. Farinazzo Bergamo Dias Martins, H. He, T. Kawaguchi, P. Zapol, H. You, D. Tripkovic, D. Strmcnik, Y. Zhu, S. Seifert, S. Lee, V. R. Stamenkovic, N. M. Markovic, *Nat. Energy* **2020**, *5*, 222–230; b) D. Zhou, P. Li, X. Lin, A. McKinley, Y. Kuang, W. Liu, W. F. Lin, X. Sun, Duan, *Chem. Soc. Rev.* **2021**, *50*, 8790–8817; c) C. Roy, B. Sebok, S. B. Scott, E. M. Fiordaliso, J. E. Sørensen, A. Bodin, D. B. Trimarco, C. D. Damsgaard, P. C. K. Vesborg, O. Hansen, I. E. L. Stephens, J. Kibsgaard, I. Chorkendorff, *Nat. Catal.* **2018**, *1*, 820–829; d) L. Lv, Z. Yang, K. Chen, C. Wang, Y. Xiong, *Adv. Energy Mater.* **2019**, *9*, 1803358.
- [17] L. Trotochaud, S. L. Young, J. K. Ranney, S. W. Boettcher, *J. Am. Chem. Soc.* **2014**, *136*, 6744–6753.
- [18] a) L. Yu, J. F. Yang, B. Y. Guan, Y. Lu, X. W. Lou, *Angew. Chem. Int. Ed.* **2018**, *57*, 172; *Angew. Chem.* **2018**, *130*, 178; b) Y. Liu, X. Liang, L. Gu, Y. Zhang, G. D. Li, X. Zou, J. S. Chen, *Nat. Commun.* **2018**, *9*, 2609; c) Y. Liang, J. Wang, D. Liu, L. Wu, T. Li, S. Yan, Q. Fan, K. Zhu, Z. Zou, *J. Mater. Chem. A* **2021**, *9*, 21785–21791; d) J. Chen, F. Zheng, S. Zhang, A. Fisher, Y. Zhou, Z. Wang, Y. Li, B. Xu, J. Li, S. Sun, *ACS Catal.* **2018**, *8*, 11342.
- [19] a) M. B. Stevens, L. J. Enman, E. H. Korkus, J. Zaffran, C. D. M. Trang, J. Asbury, M. G. Kast, M. C. Toroker, S. W. Boettcher, *Nano Res.* **2019**, *12*, 2288–2295; b) M. T. Bender, K. -S. Choi, *ChemSusChem* **2022**, *15*, e2022006; c) M. T. Bender, Y. C. Lam, S. Hammes-Schiffer, K.-S. Choi, *J. Am. Chem. Soc.* **2020**, *142*, 21538.
- [20] a) S. Barwe, J. Weidner, S. Cychy, D. M. Morales, S. Dieckhöfer, D. Hiltrop, J. Masa, M. Muhler, W. Schuhmann, *Angew. Chem. Int. Ed.* **2018**, *57*, 11460–11464; *Angew. Chem.* **2018**, *130*, 11631–11636; b) N. Zhang, Y. Zou, L. Tao, W. Chen, L. Zhou, Z. Liu, B. Zhou, G. Huang, H. Lin, S. Wang, *Angew. Chem. Int. Ed.* **2019**, *58*, 15895–15903; *Angew. Chem.* **2019**, *131*, 16042–16050.
- [21] M. Krebs, C. Wang, A. Bodach, F. Schüth, personal communication.
- [22] F. Dionigi, Z. Zeng, I. Sinev, T. Merzdorf, S. Deshpande, M. B. Lopez, S. Kunze, I. Zegkinoglou, H. Sarodnik, D. Fan, A. Bergmann, J. Drnec, J. F. Araujo, M. Gliech, D. Teschner, J. Zhu, W. X. Li, J. Greeley, B. R. Cuenya, P. Strasser, *Nat. Commun.* **2020**, *11*, 2522.
- [23] M. Gong, Y. Li, H. Wang, Y. Liang, J. Wu, J. Zhou, J. Wang, T. Regier, F. Wei, H. Dai, *J. Am. Chem. Soc.* **2013**, *135*, 8452–8455.
- [24] a) B. Chakraborty, R. Beltrán-Suito, J. N. Hausmann, S. Garai, M. Driess, P. W. Menezes, *Adv. Energy Mater.* **2020**, *10*, 2001377; b) J. N. Hausmann, R. Beltrán-Suito, S. Mebs, V. Hluchyy, T. F. Fässler, H. Dau, M. Driess, P. W. Menezes, *Adv. Mater.* **2021**, *33*, 2008823.
- [25] S. H. Shi, Y. Liang, N. Jiao, *Chem. Rev.* **2021**, *121*, 485–505.
- [26] a) D. R. Vardon, M. A. Franden, C. W. Johnson, E. M. Karp, M. T. Guarnieri, J. G. Linger, M. J. Salm, T. J. Strathmann, G. T. Beckham, *Energy Environ. Sci.* **2015**, *8*, 617–628; b) J. Rios, J. Lebeau, T. Yang, S. Lia, M. D. Lynch, *Green Chem.* **2021**, *23*, 3172–3190.
- [27] T. Wang, L. Tao, X. Zhu, C. Chen, W. Chen, S. Du, Y. Zhou, B. Zhou, D. Wang, C. Xie, P. Long, W. Li, Y. Wang, R. Chen, Y. Zou, X.-Z. Fu, Y. Li, X. Duan, S. Wang, *Nat. Catal.* **2022**, *5*, 66–73.

Manuscript received: October 27, 2022

Accepted manuscript online: November 28, 2022

Version of record online: December 16, 2022